Cite this article
Jafari S, Bozorg-Haddad O, Ashofteh PS and Loáiciga HA (2021)
Uncertainties in agricultural water supply under climate change: Aidoghmoush basin, Iran.
Proceedings of the Institution of Civil Engineers – Water Management **174(3)**: 120–133,
https://doi.org/10.1680/jwama.19.00032

Research Article
Paper 1900032
Received 28/05/2019;
Accepted 08/01/2021;
Published online 02/03/2021

Keywords: earth dams/hydrology & water resource/risk & probability analysis

Water Management

ice Publishing

Uncertainties in agricultural water supply under climate change: Aidoghmoush basin, Iran

1 **Saba Jafari** MSc
MSc graduate, Department of Irrigation & Reclamation Engineering, Faculty of Agricultural Engineering & Technology, College of Agriculture & Natural Resources, University of Tehran, Karaj, Iran

2 **Omid Bozorg-Haddad** PhD
Distinguished Professor, Department of Irrigation & Reclamation Engineering, Faculty of Agricultural Engineering & Technology, College of Agriculture & Natural Resources, University of Tehran, Karaj, Iran (Orcid:0000-0001-6607-9581) (corresponding author: obhaddad@ut.ac.ir)

3 **Parisa-Sadat Ashofteh** PhD
Assistant Professor, Department of Civil Engineering, University of Qom, Qom, Iran

4 **Hugo A. Loáiciga** PhD
Professor, Department of Geography, University of California, Santa Barbara, CA, USA




The planning of future supplies of agricultural water is beset by uncertainties stemming from inaccuracies in general circulation models, assumed greenhouse gases emissions scenarios (GHGESs), imperfect models employed for estimating reservoir inflows and approximate methods for estimating agricultural water demand. The uncertainty of providing agricultural water under climate change was assessed, relying on simulations involving baseline (1971–2000) and future periods (2040–2069 and 2070–2099). Climatic variables were simulated using six atmosphere–ocean general circulation models (AOGCMs) driven by GHGESs A2 and B2 in the Aidoghmoush basin, Iran. Projection of reservoir inflow was performed using the IHACRES model and artificial neural network (ANNs). Agricultural water demand was calculated using the FAO–Penman–Monteith and Hargreaves-Samani (HS) methods. Eight modelling scenarios were considered based on combinations of AOGCMs, GHGESs, reservoir inflow and agricultural water demand projections. Reservoir operation rules were calculated with a particle swarm optimisation algorithm. The results show that agricultural water demand will increase in future periods compared with the baseline period. The operation rule derived from the combination of the HS and ANN models (under GHGES A2) showed the best performance in 2040–2069 by achieving the highest reliability (93%) of water supply. The operation rule derived from the combination of HS and ANN models (under GHGES B2) achieved the highest reliability (95%) of water supply in 2070–2099. The results provide adjusted reservoir operation rules under uncertainty caused by climate change and related impacts on water resources management.

Notation

A_C	area under crop cultivation
D_i	volume of agricultural water demand during period i
ET_{C_i}	crop evapotranspiration in month i
ET_0	reference evapotranspiration
ET_{0_i}	reference evapotranspiration in month i
e_a	actual vapour pressure
e_s	saturation vapour pressure
$e_s - e_a$	saturation vapour pressure deficit
G	soil heat flux density
IR_i	net irrigation requirement in month i
i	operation period
K_{C_i}	crop coefficient during month i
Max $D_{i=1}^{n}$	maximum demand volume during operation periods
N	number of atmosphere–ocean general circulation models (AOGCMs)
n	number of operation periods
P_{eff_i}	effective precipitation in month i
P_i	projected time series of precipitation for month i
$P_{obs,i}$	time series precipitation observed in month i of baseline period
R	correlation coefficient
R_a	solar radiation at top of atmosphere for a given latitude in terms of equivalent evaporation

R_i	volume of water release from reservoir during period i
R_n	net radiation at crop surface
T	mean daily air temperature at 2 m height
T_{ave}	average daily air temperature
T_i	projected time series of temperature for month i
T_{obs}	observed temperature
$T_{obs,i}$	time series of temperature observed in month i of baseline period
$\bar{T}_{GCM,base,i}$, $\bar{P}_{GCM,base,i}$	30-year temperature and precipitation averages, respectively, simulated with the six AOGCMs during the baseline period for month i
$\bar{T}_{GCM,fut,i}$, $\bar{P}_{GCM,fut,i}$	30-year temperature and precipitation averages, respectively, simulated with general circulation models in future periods for month i
TR	difference between maximum and minimum daily air temperature
U_2	wind speed at 2 m height
V_i	volume of water demand in month i
$WP_{i,j}$	weight assigned to simulation of precipitation with model j for month i
$WT_{i,j}$	weight assigned to simulation of temperature with model j for month i
γ	psychrometric constant
Δ	slope of vapour pressure curve
ΔP_i	precipitation ratio
$\Delta P_{i,j}$	difference between long-term average monthly precipitation simulated with the jth AOGCM in the baseline period and the average long-term monthly precipitation observed in month i
ΔT_i	temperature difference
$\Delta T_{i,j}$	difference between long-term average monthly temperature simulated with the jth AOGCM in the baseline period and the long-term average monthly temperature observed in month i

1. Introduction

Agricultural water use exceeds all other water uses in many semi-arid regions. The future supply of agricultural water may be imperilled by climate change (Baede *et al.*, 2001; Pachauri and Reisinger, 2007), by economic growth and concomitant agricultural water use and by the complexities of water storage and distribution systems (Ashofteh, 2015; Ashofteh *et al.*, 2017; Farhangi, 2010).

This paper presents a methodology for extracting adjusted reservoir operation rules under uncertainty caused due to climate change. Future climate change impacts are difficult to predict with accuracy, especially at regional scales (of the order of 10^4–10^5 km^2). For this reason, it is noteworthy that this paper presents a methodology for evaluating a range of probable climate change effects on reservoir operation rules to assist water users in developing adaptive strategies. Previous works pertinent to the contents of this paper are briefly reviewed next.

Minville *et al.* (2008) projected the impact of climate change on the hydrology of the Chute-du-Diable watershed in Quebec, Canada. The use of ten equally weighted climate projections from a combination of five general circulation models (GCMs) and two greenhouse gas emissions scenarios (GHGESs) provided an uncertainty envelope of future hydrologic variables. Their results indicated a 1–14°C increase in seasonal temperature and a change in seasonal precipitation of −9% to +55%. Abbaspour *et al.* (2009) employed a hydrologic model of Iran to study the impact of future climate on the country's water resources. The hydrologic model was created with the soil and water assessment tool. Climate scenarios for 2010–2040 and 2070–2100 were generated with the Canadian global coupled model (CGCM3.1) for GHGESs A1B, B1 and A2, which were downscaled for 37 climate stations across the country. Li *et al.* (2010) examined the potential impacts of future climate change on streamflow and reservoir operation performance in North American basins. GHGESs A2 and B2 were applied to project daily precipitation and temperature with the CGCM2 model for dynamic reservoir modelling based on basin hydrology. The results demonstrated that future climate variation and change may bring more high peak streamflow occurrences. More abundant water resources and current reservoir operation rules could provide a high reliability for drought protection and flood control (Asgari *et al.*, 2016; Soltanjalili *et al.*, 2011). Warren and Holman (2012) evaluated the effects of climate change on the water resources of the city of Birmingham, UK. Baseline and future climate projections were generated with the UK Climate Projections 2009 and a daily soil water balance model was applied. The results showed that climate change will decrease the reliability of the system. Fallah-Mehdipour *et al.* (2014) analysed different artificial intelligence tools for modelling water recourses and extracted their governing rules. Ashofteh *et al.* (2015) assessed the risk of increasing water demand for irrigated crops in an irrigation network located downstream of Aidoghmoush dam in East Azerbaijan, Iran, due to climate change for the period 2026–2039. The Bayesian method was implemented to assess the uncertainty of atmosphere–ocean general circulation models (AOGCMs) and the FAO–Penman–Monteith (FPM) method was applied to calculate future evapotranspiration. Their results showed that changing crop patterns could be one of the strategies for adapting to climate change in the region. Jahandideh-Tehrani *et al.* (2015) studied the effects of climate change on the performance of hydropower reservoirs and demonstrated the benefits of using optimisation modelling to adapt to the effects of climate change. Masood and Takeuchi (2016) reported on the effects of climate change and its consequences on the future management of water resources in the Magna basin, Bangladesh. The impacts of climate change were assessed with the high-resolution MRI-AGCM3.2S and the GHGES A1B in a baseline period (1979–2003),

the near-future (2015–2039) and the far-future (2075–2099). Their results showed that (*a*) the projected maximum increment of mean annual precipitation (runoff) would be +23% (+34%) and +31% (+39%) in the near-future and the far-future periods, respectively and (*b*) the projected increment of the median value of monthly discharges at the basin outlet would be significantly high in the wet season (May–July), ranging from 38–44% and 25–104% in the near-future and the far-future periods, respectively. Xing-Guo *et al.* (2017) assessed the impacts of climate change on agricultural water demand in the North China plain. The GCMs projected that, by the 2050s, the increased crop water demand and elevated evapotranspiration resulting from global warming would reduce water resources surplus by about 4–24% and significantly increase the irrigation water demand during growth periods.

Previous studies have projected the impacts of climate change on water resources, agricultural water demand and reservoir operation performance. Some of the studies have accounted for uncertainties in their projections. In this work, the effects of climate change on agricultural water demand were projected and reservoir operation policies to cope with such effects were developed. The projections provided in this paper are innovative as, compared with previous studies, a more general set of uncertainties was considered. Specifically, uncertainties in GHGESs, AOGCMs, water demand and simulation models for water resources were considered. These uncertainties were applied to the projection of climate change impacts and reservoir operation in the Aidoghmoush basin in East Azerbaijan province, Iran.

2. Methods

This section introduces the study area and the future climate scenarios and the models and methods for estimating reservoir inflow and agricultural demand. The reservoir operation rules corresponding to the different modelling scenarios are explained. A flowchart of the methodology is shown in Figure 1.

2.1 The study area

The study area was Aidoghmoush basin, located in East Azerbaijan province, Iran. The basin has an area of 1802 km^2, within 46°52′E and 47°45′E longitude and 36°43′N and 37°26′N latitude. The 80-km long Aidoghmoush River originates in the Gorgerd mountains and flows to the Ghezel-Ozan River. The average discharge of the Aidoghmoush River is almost 170×10^6 m^3 annually (Ashofteh *et al.*, 2015). The geographic location of the Aidoghmoush reservoir is shown in Figure 2.

The study's region climate is semi-arid with an average annual temperature of 11.6°C and average annual precipitation of 336.3 mm. In this study, the period 1971–2000 was used as a baseline, with the average temperature and precipitation of this period serving for projecting the climatic variables in two future periods (2040–2069 and 2070–2099). The average annual water demand for agriculture in the basin is 11.61×10^6 m^3. The crops cultivated in the area are wheat, barley, alfalfa, soybeans, forage corn, maize, potatoes and walnuts.

2.2 Modelling scenarios

Eight modelling scenarios (MS1–MS8) were generated for the first future period (2040–2069 (2050s)) and the second future period (2070–2099 (2080s)). As shown in Table 1, these

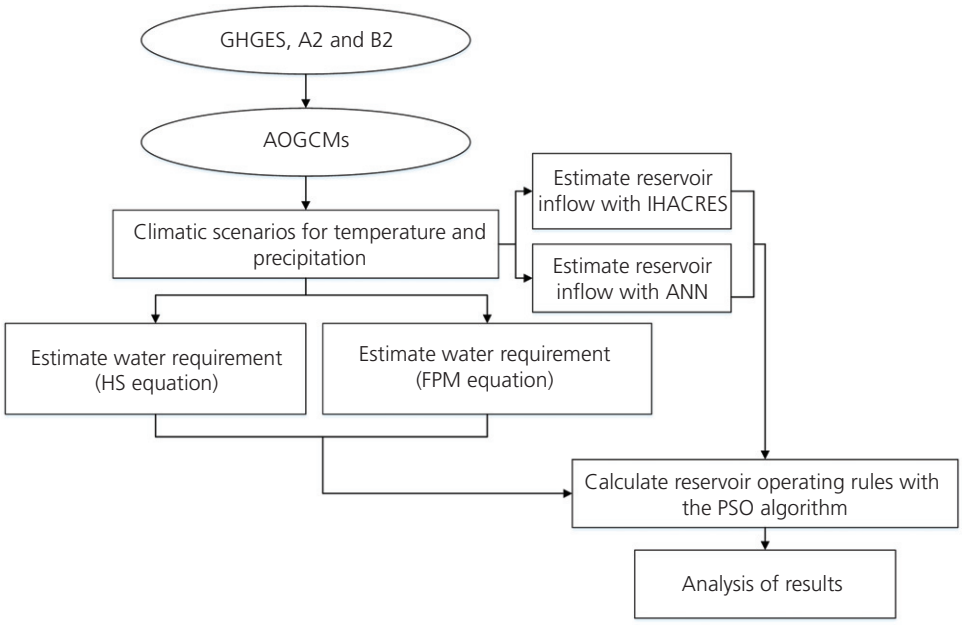

Figure 1. Flowchart of methodology

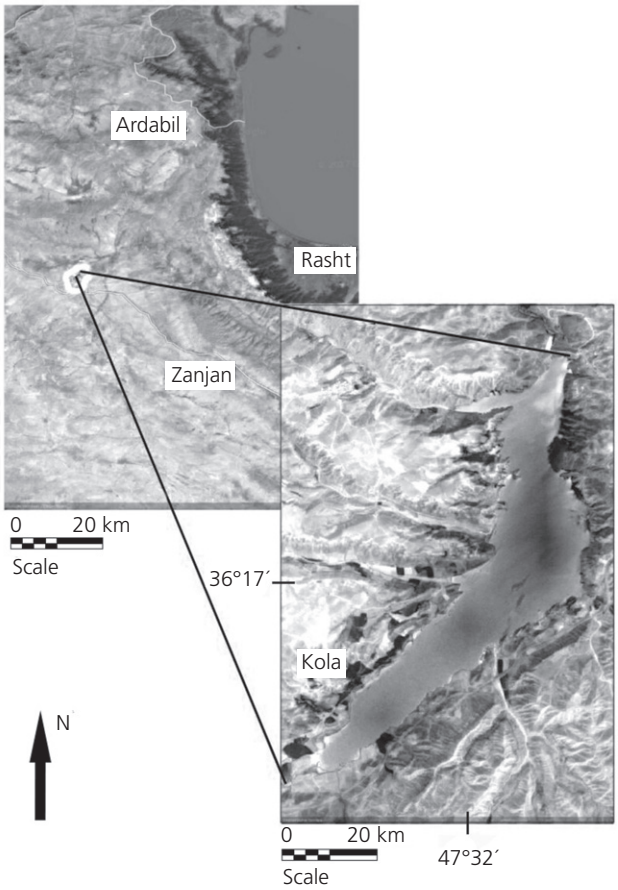

Figure 2. Geographic location of Aidoghmoush reservoir

scenarios correspond to different combinations of GHGESs (A2 and B2), two methods of estimating agricultural demand (i.e. the FPM method and the Hargreaves–Samani (HS) method), two models to project reservoir inflow (i.e. Identification of unit hydrographs and component flows from rainfall, evaporation and streamflow (IHACRES) or artificial neural network (ANN)).

2.3 Uncertainties

The uncertainties considered in this study were the uncertainty associated with AOGCMs, the uncertainty of GHGESs, the uncertainty of water demand estimation and the uncertainty of water resources simulation models. These uncertainties are explained next.

Table 1. Modelling scenarios used for both future time periods (2040–2069 and 2070–2099)

Modelling scenario	Estimation method	GHGES
MS1	ANN–FPM method	A2
MS2	ANN-Hargreaves	A2
MS3	IHACRES–FPM method	A2
MS4	IHACRES-Hargreaves	A2
MS5	ANN–FPM method	B2
MS6	ANN-Hargreaves	B2
MS7	IHACRES–FPM method	B2
MS8	IHACRES-Hargreaves	B2

2.3.1 AOGCMs

wThe uncertainties associated with six AOGCMs are illustrated with the average monthly precipitation and temperature projected by six AOGCMs for the baseline and future periods extracted from the Intergovernmental Panel for Climate Change (IPCC) website according to the third assessment report of the IPCC (IPCC, 2001). The AOGCMs applied in this study were HadCM3, CGCM2, CCSR-NIES, ECHAM4, GFDL-R30 and CSIRO-MK2. Therefore, six of the seven GCMs included in the IPCC third assessment report (IPCC, 2001) were evaluated in this study. The NCAR-DOE PCM model was not included here due to its unsuccessful performance in simulating rainfall and temperature parameters during the baseline period. Monthly precipitation and temperature were calculated with the AOGCMs to construct the monthly average temperature difference (ΔT_i) and the precipitation ratio (ΔP_i) (Loáiciga *et al.*, 2000; Wilby and Harris, 2006) as follows.

$$1.\quad \Delta T_i = \bar{T}_{\mathrm{GCM,fut},i} - \bar{T}_{\mathrm{GCM,base},i}$$

$$2.\quad \Delta P_i = \frac{\bar{P}_{\mathrm{GCM,fut},i}}{\bar{P}_{\mathrm{GCM,base},i}}$$

In Equations 1 and 2, which $1 \le i < 12$ denotes the index for the 12 months of the year, $\bar{T}_{\mathrm{GCM,fut},i}$ and $\bar{P}_{\mathrm{GCM,fut},i}$ are, respectively, the 30-year temperature and precipitation averages simulated with the GCMs in the future periods for month i and $\bar{T}_{\mathrm{GCM,base},i}$ and $\bar{P}_{\mathrm{GCM,base},i}$ are, respectively, the 30-year temperature and precipitation averages simulated with the six AOGCMs during the baseline period for each month i. The temperature difference in Equation 1 was added to the historic temperature in the baseline period to create the future projected temperature. The precipitation ratio in Equation 2 was multiplied by the historic precipitation in the baseline period to create the future projected precipitation, as described below.

The weight of each AOGCM model was obtained based on the mean observed temperature–precipitation approach according to Equations 3 and 4 (Ashofteh *et al.*, 2014)

$$3.\quad \mathrm{WT}_{i,j} = \frac{(1/\Delta T_{i,j})}{\sum_{j=1}^{N}(1/\Delta T_{i,j})}$$

$$4.\quad \mathrm{WP}_{i,j} = \frac{(1/\Delta P_{i,j})}{\sum_{j=1}^{N}(1/\Delta P_{i,j})}$$

in which $WT_{i,j}$ is the weight assigned to simulation of temperature with model j for the ith month, $WP_{i,j}$ is the weight assigned to the simulation of precipitation with model j for the ith month, N is the number of AOGCMs, $\Delta T_{i,j}$ is the difference between the long-term average monthly temperature simulated with the jth AOGCM in the baseline period and the long-term average monthly temperature observed in the ith month, and $\Delta P_{i,j}$ is the difference between the long-term average monthly precipitation simulated with the jth AOGCM in the baseline period and the average long-term monthly precipitation observed in the ith month.

Data including time series of monthly temperature and precipitation (ΔT_i) and (ΔP_i) and monthly weights of each model per were input to the SimLab model to generate 100 random samples of temperature and precipitation projections for the ith month by means of Monte Carlo simulation. Equations 5 and 6 were applied to calculate the time series of future temperature and precipitation, respectively

$$T_i = T_{\text{obs},i} + \Delta T_i \quad (5)$$

$$P_i = P_{\text{obs},i} \times \Delta P_i \quad (6)$$

in which $T_{\text{obs},i}$ and $P_{\text{obs},i}$ are the time series of temperature and precipitation observed in month i of the baseline period, respectively, and T_i and P_i are the projected time series of temperature and precipitation for month i, respectively (Ashofteh, 2015).

2.3.2 GHGESs

The IPCC GHGESs were constructed to explore future developments in the global environment with reference to the emissions of greenhouse gases (GHGs) that contain various driving processes of climate change, including population growth and socioeconomic development. The IPCC defines scenarios labelled A1, A2, B1 and B2, describing the relations between the forces driving GHGs and their evolution during the twenty first century and globally. This work relied on GHGESs A2 and B2 applied to the six AOGCMs. GHGESs A2 and B2 were introduced in the IPCC third assessment report (IPCC, 2001). GHGES A2 postulates the highest emission of GHGs, thus constituting the most pessimistic scenario. In contrast, GHGES B2 envisions relatively low GHGs emissions and is the most optimistic scenario in this respect. The two GHGES selected for this study provide a wide range of expected impacts of climate change.

2.3.3 Simulation of rainfall–runoff

The IHACRES model has accurate predictive skill while requiring fewer input data than other hydrologic models; it also has simple logic and algorithmic simplicity to calculate runoff. For these reasons, it was chosen as one of the rainfall–runoff models in this study. The other runoff-predicting method applied was an ANN model, which predicts peak reservoir inflows (streamflow) in snow-fed basins such as the Aidoghmoush more accurately than IHACRES. The IHACRES and ANN models were used to make projections of reservoir inflow.

- The IHACRES model was introduced by Jakeman and Hornberger (1993). It is a lumped-simulation model that predicts runoff for given climatic inputs (Besaw *et al.*, 2010). IHACRES comprises a non-linear loss module and a linear unit hydrograph module, which, respectively, calculate losses of precipitation and convert effective precipitation into runoff (Croke *et al.*, 2005; McIntyre and Al-Qurashi, 2009).
- The ANN model used in this study operates on temperature and precipitation data. It divides the data into two sets, one for training (calibration) and one for testing (of predictive accuracy). Representative patterns must be present in the entire dataset to improve predictive learning. The ANN structure features three layers, each with separate functions – the input layer for the distribution of data in the network, the middle (hidden) layer for information processing and the output layer, which performs information processing and output display (Bani-Habib *et al.*, 2010). The ANN input data for this study were observed temperature, precipitation and runoff, and future temperature and precipitation. The ANN predicted runoff data in the future periods (runoff projections).

2.3.4 Calculation of irrigation requirements and estimation of water demand downstream of the reservoir

The reference evapotranspiration (ET_0) is often used to calculate the (actual) evapotranspiration of crops under actual soil moisture conditions. The American Society of Civil Engineers (ASCE) defined evapotranspiration (synonymously with consumptive use) as the quantity of water transpired by plants during growth or retained in plant tissue, plus the moisture evaporated from the surface of the soil and the vegetation (Jensen, 1974). The Food and Agricultural Organization (FAO) defined ET_0 as the evapotranspiration rate from a surface covered with a hypothetical grass with specific characteristics, not short of soil water (FAO, 1998). Later, ASCE defined ET_0 as the evapotranspiration rate from a uniform surface of dense, actively growing vegetation having a specified height and surface resistance, not short of soil water, and representing an expanse of at least 100 m of the same or similar vegetation (Allen *et al.*, 2005). The 'hypothetical grass with specific characteristics' of the FAO (FAO, 1998) corresponds to ASCE's 'uniform surface of dense, actively growing, vegetation having specified height and surface resistance' (Allen *et al.*, 2005). Both definitions of ET_0 are synonymous for the purpose of estimating the

evapotranspiration by an actively growing crop uniformly and densely covering land not short of soil water. The reference evapotranspiration defined by FAO (1998) and ASCE (Allen *et al.*, 2005) must not be confused with the potential evapotranspiration (PET), originally defined by Thornthwaite (1948), who introduced PET for climate classification and defined it as the amount of water that would transpire and evaporate under ideal conditions of soil moisture and vegetation. Penman (1956) adapted Thornthwaite's definition of PET to agricultural meteorology by defining it as the amount of water transpired in unit time by a short green crop, completely shading the ground or of uniform height and never short of water.

In this study, estimations of the reference evapotranspiration (ET_0) and the evapotranspiration of crops were made using the FPM and HS methods. Previous studies have shown that the accuracy of the FPM method in calculating ET_0 is closer to the values measured by lysimeters than other methods, and the FAO has proposed this equation as the standard method of calculating ET_0. Due to its high accuracy, the FPM was adopted in this study for estimating the irrigation requirement. In this study, the climatic parameters simulated in future periods were rainfall and temperature. Therefore, high-precision models with the least number of input parameters should be used to estimate evapotranspiration. The HS method has shown suitable accuracy in predicting reference evapotranspiration. It requires only surface air temperature and solar radiation at the top of the atmosphere to calculate the irrigation water requirement.

2.3.4.1 The FPM method

The FPM method is commonly employed to estimate reference evapotranspiration (Allen *et al.*, 1998, 2005). For a short crop

$$7.\quad ET_0 = \frac{[0.408\Delta(R_n - G)] + \{\gamma[900/(T+273)]U_2(e_s - e_a)\}}{\Delta + \gamma(1 + 0.34U_2)}$$

in which ET_0 is measured in mm/day, R_n is the net radiation at the crop surface ((MJ/m^2)/day), G is the soil heat flux density ((MJ/m^2)/day), T is the mean daily air temperature at 2 m height (°C), U_2 is the wind speed at 2 m height (m/s), e_s is the saturation vapour pressure (kPa), e_a is the actual vapour pressure (kPa), $e_s - e_a$ is the saturation vapour pressure deficit (Pa), $\Delta$is the slope of the vapour pressure curve (kPa/°C) and γ is the psychrometric constant (kPa/°C).

2.3.4.2 The HS method

The HS method is a temperature- and radiation-based empirical formula that has been applied to calculate ET_0. The formula is (Hargreaves and Samani, 1985)

$$8.\quad ET_0 = 0.0023R_a(T_{ave} + 17.8)\sqrt{TR}$$

in which TR is the difference between the maximum and minimum daily air temperature (°C), T_{ave} is the average daily air temperature in (°C), R_a is the solar radiation at the top of the atmosphere for a given latitude in terms of equivalent evaporation (mm/day) and ET_0 is the reference evapotranspiration in (mm/day). The daily ET_0 values are added to calculate the monthly ET_0.

2.3.4.3 Calculating crop water use

Crop evapotranspiration (ET_C) is estimated by multiplying the reference evapotranspiration by a crop coefficient (K_C) (Doorenbos and Pruitt, 1984)

$$9.\quad ET_{C_i} = K_{C_i} \times ET_{0_i}$$

where ET_{C_i} is the crop evapotranspiration in month i, ET_{0_i} is the reference evapotranspiration in month i and $K_{C_i}$is the crop coefficient during month i.

The effective precipitation that generates runoff was calculated with the Soil Conservation Service and applying Cropwat software (Smith, 1992) as

$$10.\quad P_{eff_i} = P_i/125 \times (125 - 0.2P_i) \quad P_i \leq 250 \text{ mm}$$

$$11.\quad P_{eff_i} = 125 + 0.1P_i \quad P_i > 250 \text{ mm}$$

in which P_{eff_i} is the effective precipitation (mm) in month i and P_i is the precipitation in month i.

The monthly irrigation requirement was calculated using

$$12.\quad IR_i = ET_{C_i} - P_{eff_i} \quad IR_i \geq 0$$

in which IR_i is the net irrigation requirement (mm) in month i. In some cases it may be appropriate to divide the IR_i calculated using Equation 12 by the water-application efficiency (a fractional number) and adding to the result the amount of water lost during conveyance to the cropland. Equation 12 assumes a water-application efficiency of 1 and no conveyance losses.

The volume of water used by a crop when there is no shortage of soil water was calculated from

$$13.\quad V_i = A_C \times IR_i$$

where A_C is the area under cultivation of a crop and V_i is the volume of water demand in month i.

2.4 Optimisation and application of the particle swarm optimisation (PSO) algorithm

The PSO algorithm (introduced by Kennedy and Eberhart (1995)) was employed to optimise reservoir operation. PSO is inspired by the social behaviour of animals, fishes or birds that exhibit communal and associative life. The PSO algorithm starts with the generation of random populations of tentative solutions, or particles, each of which is made up of a set of values for the decision variables. The value of the objective function is calculated for each particle at any position of the solution space. After this calculation, the direction of movement of any particle is determined based on its current position, the best position it has previously occupied and the positions and characteristics of one or more other particles in the population. Evaluation of the objective function of particles and determination of improved positions is carried out in every iteration for all particles in all populations. The populations of particles are improved from one iteration to the next until a convergence criterion is reached. The best particle upon convergence represents the optimal solution to the problem being solved.

The objective function of the reservoir operation problem for irrigation water supply is given by

$$\text{14.} \quad \text{Minimise the OF} = \sum_{i=1}^{n} \left(\frac{D_i - R_i}{\text{Max } D_{i=1}^{n}} \right)^2$$

in which OF is the objective function quantifying the relative water deficit during the operation periods (monthly periods), i is the index for the operation period, n is the number of operation periods, D_i is the volume of agricultural water demand during period i, Max $D_{i=1}^{n}$ is the maximum demand volume during the operation periods and R_i is the volume of water release (the decision variables) from the reservoir during period i.

3. Results and discussion

3.1 Performance of the AOGCMs in the simulation of climate variables in the period 1971–2000

The values of long-term average climate variables simulated with the AOGCMs were compared with the values of long-term average observed variables at the representative station within the basin over the baseline period (1971–2000). The comparison was based on performance criteria expressed by the correlation coefficient (R), root mean square error (RMSE) and the mean absolute error (MAE). As shown in Table 2, the HadCM3 model provided the best performance in simulating climatic variables under GHGESs A2 and B2. Specifically, HadCM3 simulated precipitation and temperature with R values of 99.6% and 91% (under GHGES A2) and 99.5% and 87% (under GHGES B2), respectively.

3.2 Time series of temperature and precipitation in future periods

Figures 3(a) and 3(b) shows that the projected average long-term monthly temperature in the second future period under GHGES A2 was higher than the projected average temperature in the first future period. The long-term average monthly temperature in the future periods was also predicted to be higher than the temperature in the baseline (observational) period. Furthermore, Figures 3(c) and 3(d) show that the same patterns applied to GHGES B2 in most of the months. It is also evident from Figure 3 that the long-term average monthly temperature in future periods under scenario A2 will be higher than the long-term average monthly temperature under scenario B2.

Table 2. Performance of AOGCMs in simulating temperature and precipitation by comparison with observed variables under GHGESs A2 and B2

	Temperature			Precipitation		
Model	*R*: %	RMSE: °C	MAE: °C	*R*: %	RMSE: mm	MAE: mm
GHGES A2						
HadCM3	99.6	1.18	1.00	91	8.66	6.78
CCSR-NIES	99.6	7.89	7.84	67	19.12	14.31
CSIRO-MK2	99.1	1.34	1.25	77	14.61	10.96
CGCM2	97.9	2.50	1.94	77	52.63	36.13
GFDL-R30	99.4	3.74	3.14	97	12.30	10.66
ECHAM4	98.9	2.37	1.72	90	20.21	16.75
GHGES B2						
HadCM3	99.5	1.21	0.99	87	10.04	7.64
CCSR-NIES	99.5	7.90	7.85	69	19.03	14.19
CSIRO-MK2	99.2	1.30	1.21	80	13.87	10.19
CGCM2	98.1	2.46	1.89	75	52.96	35.89
GFDL-R30	99.5	3.72	3.10	96	10.05	8.58
ECHAM4	98.9	2.37	1.72	90	20.21	16.75

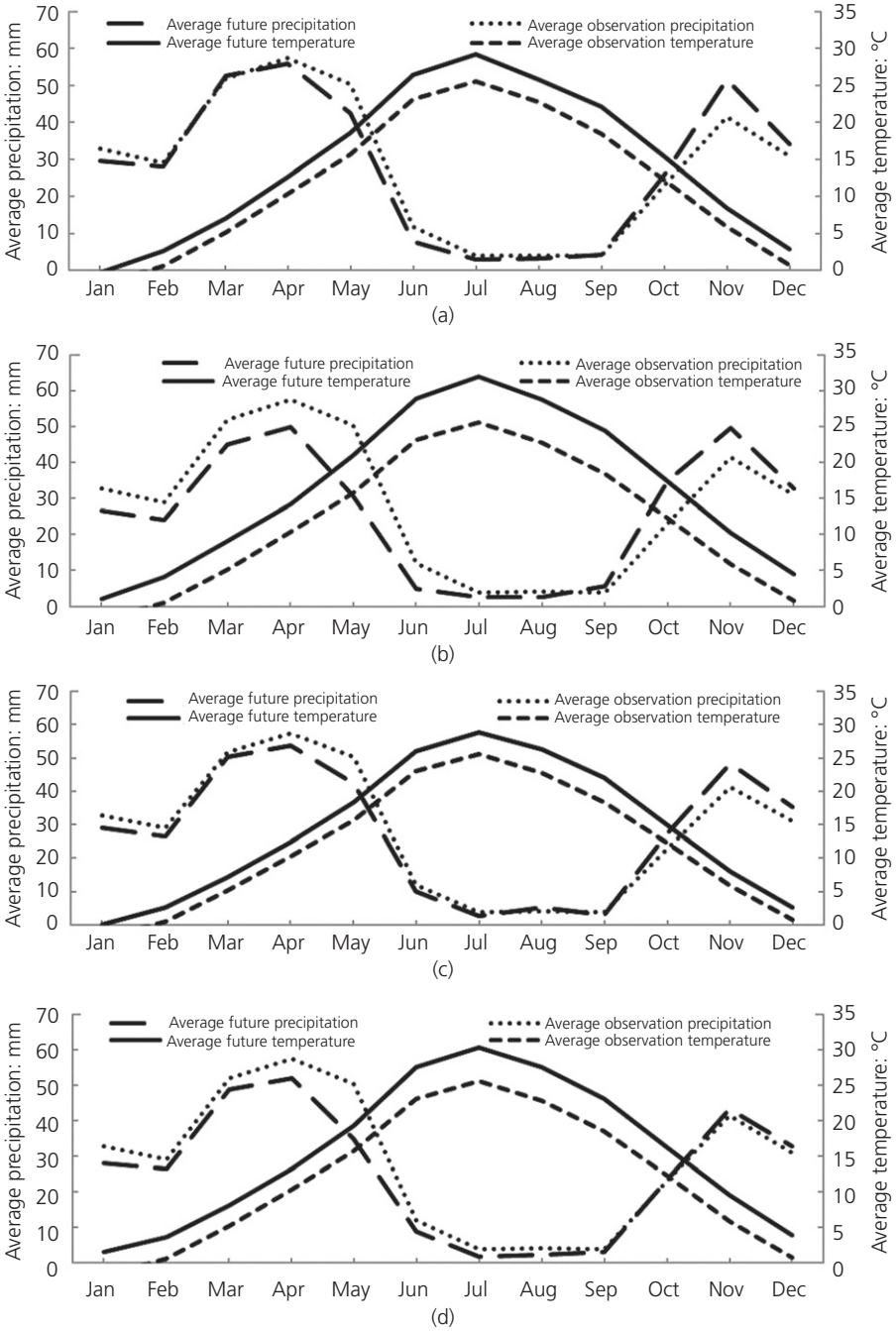

Figure 3. Comparison of the projected long-term average monthly precipitation and temperature in (a) the first future period (2040–2069) and (b) the second future period (2070–2099) with the monthly average precipitation and temperature observed in the baseline period (1971–2000) under GHGES A2. Comparison of the projected long-term average monthly precipitation and temperature in (c) the first future period (2040–2069) and (d) the second future period (2070–2099) compared with the monthly average precipitation and temperature observed in the baseline period (1971–2000) under GHGES B2

3.3 Simulation of reservoir inflow

3.3.1 IHACRES model

The time series of average monthly reservoir inflows in the two future periods (2040–2069 and 2070–2070) under GHGESs A2 and B2 projected with the IHACRES model are presented in Figure 4. Figure 4 The figure shows that, under both GHGESs (A2 and B2), the reservoir inflow in future periods will be significantly less than the observed inflow in the baseline period. Furthermore, the inflow in the second future

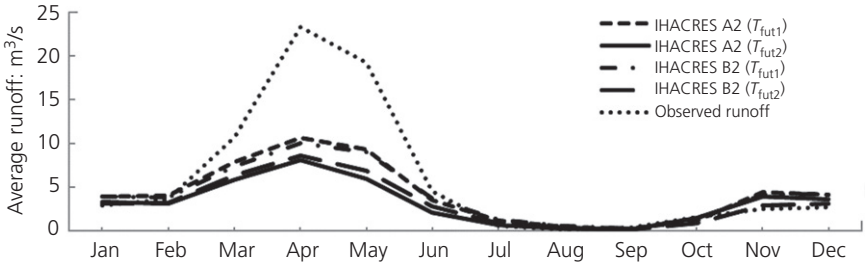

Figure 4. Comparison of observed reservoir inflow with long-term mean monthly reservoir inflow under GHGESs A2 and B2 simulated with IHACRES

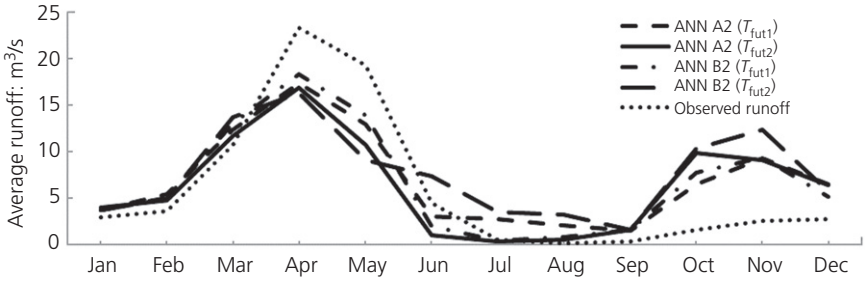

Figure 5. Comparison of observed average monthly reservoir inflow with long-term average monthly reservoir inflow simulated with ANN under GHGESs A2 and B2

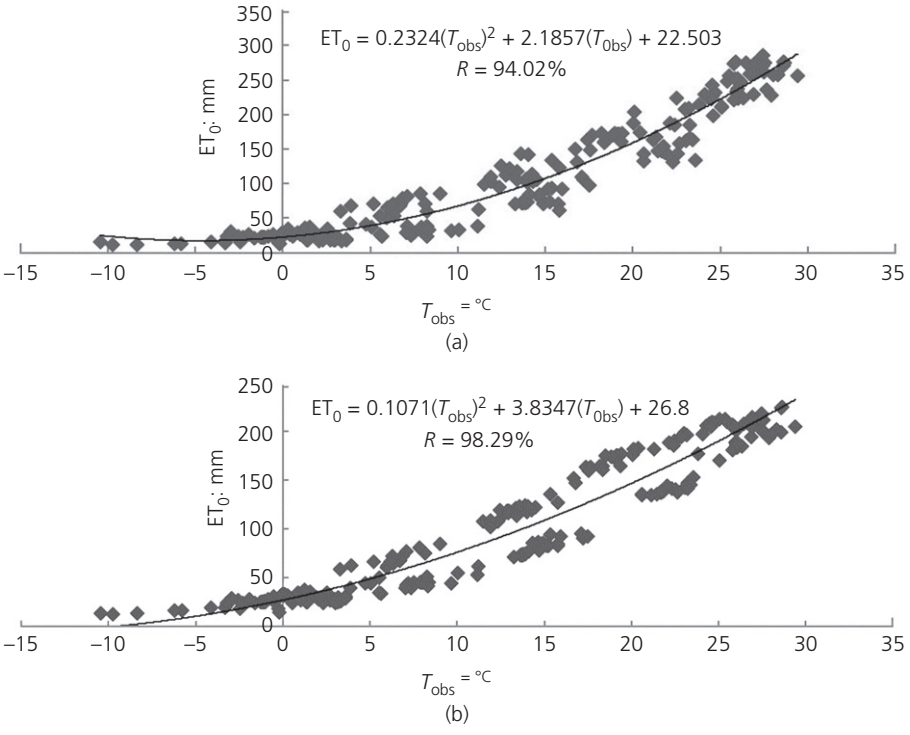

Figure 6. Regressions between monthly ET_0 and T_{obs} in the baseline period (1971–2000) based on (a) the FPM method and (b) the HS method

period will be smaller than that of the first future period, so that the sum of the average long-term monthly runoff in the first and second future period under GHGES A2 would be decreased by 29% and 46.61%, respectively, and under GHGES B2 would be decreased by 31% and 45.56% compared with the baseline period. These projections suggest future declining reservoir inflows.

3.3.2 ANN model runoff projections

Figure 5 shows the average monthly reservoir inflows projected with the ANN model in the two future periods under GHGESs A2 and B2. It is evident that April, May, and June runoff projected by the ANN model under GHGESs A2 and B2 is less than the observed runoff in the baseline period. The sum of average monthly runoff under A2 in the future periods would increase by 74.15% and under B2 it would increase by 49.12% compared with the inflow observed in the baseline period. In the second future period, reservoir inflow will increase by 41.6% and 33.27% under A2 and B2 compared with the baseline period, respectively.

3.4 Estimation of irrigation requirement and water demand

A regression equation between temperature and ET_0 in the baseline period was developed (Ashofteh *et al.*, 2015) and employed to project ET_0 in future periods. This was necessary because of a lack of data for calculating ET_0, such as relative humidity, net radiation (R_n), wind speed at 2 m height (U_2) and so on in the future periods.

Figure 6 shows the ET_0 calculated with Equation 7 (the FPM method) and Equation 8 (the HS method). The correlation coefficients of the regression between the ET_0 and observed temperature (T_{obs}) for the FPM and HS method were determined to be 94.02% and 92.29%, respectively, which are acceptable. Subsequently, projected temperatures in the two future periods were input to the developed regression to project the future ET_0.

Table 3 lists four combinations of GHGESs A2 and B2 and the FPM and HS equations employed to project agricultural water demand. Figures 7(a)–7(d) show the calculated average monthly water demands in the baseline and future periods. Figure 7(a) shows that the increase in water demand in future periods would be largest in June, July, August and September compared with the baseline period base for case 1 (FPM method and GHGES A2). This case suggests a significant future increase in water demand in the summer. Compared with the baseline period, the increases for the first and second future periods would be 20.3% and 39.6%, respectively. Figure 7(b) shows that the peak increase in agricultural water demand for case 2 (FPM method and GHGES B2) for the future period would be in September, not in August as projected under case 1. Compared with the baseline period, the increases in water demand under case 2 in the first and second future periods would be 18.1% and 35.8%, respectively. Figure 7(c) shows that, compared with the baseline period, the increases in water demand in the first and second future periods would be 19% and 36.7%, respectively, under case 3 (HS method and GHGES A2). This case shows lower percentage increases in water demand compared with case 1. Figure 7(d) shows the projections for case 4 (HS method and GHGES B2): the increase in water demand would decline compared with case 3, to 16.6% for the first future period and 32.7% for the second future period.

Table 3. Cases for calculation of agricultural water demand

	GHGES used for estimating ET_0 in future period	ET_0 formula for baseline period
Case 1	A2	FPM method
Case 2	B2	FPM method
Case 3	A2	HS method
Case 4	B2	HS method

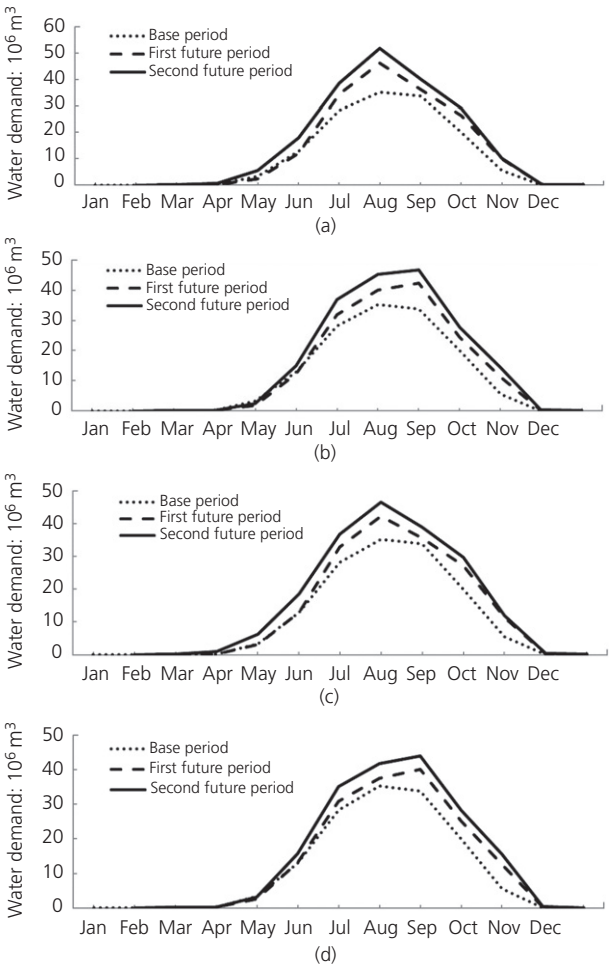

Figure 7. Average long-term monthly water demand in the baseline and future periods for different cases for calculating water demand (see Table 3): (a) case 1; (b) case 2; (c) case 3; (d) case 4

3.5 Optimisation and performance criteria

Optimised reservoir operation to meet future agricultural water demand was calculated using the PSO model. Optimised reservoir operation was calculated independently for the eight modelling scenarios listed in Table 1 for the two future periods. Figure 8 shows the results of average monthly reservoir water release calculated for MS1, MS2, MS3 and MS4 (corresponding to GHGES A2) in the first future period (2040–2069). The figure shows that in the first future period and under GHGES A2, the ANN model performed better than IHACRES in projecting monthly reservoir inflows. The modelling scenarios using the HS method showed slightly better performance than those employing the FPM method. It is concluded that MS2 would meet 92.68% of the future water demand and this scenario showed the best performance. MS1 is the second best performing scenario, meeting 91.19% of the water demand. MS4 would meet 51.42% of the water demand. MS3 is the worst performing scenario, meeting only 49.65% of the water demand.

Figure 9 shows the monthly reservoir water releases corresponding to MS5, MS6, MS7 and MS8 (corresponding to GHGES B2) in the first future period (2040–2069). Figure 9 shows similar trends to those in Figure 8, except that the peak water release to meet increasing demand shifts from July to August. The best performing scenario is MS6, meeting 88.36% of the future water demand. MS5, MS8 and MS7 would meet 86.46%, 52.65% and 48.29% of the water demand, respectively.

Figure 10 shows the average monthly reservoir water releases for MS1, MS2, MS3 and MS4 in the second future period under GHGES A2. It is evident from the figure that the water demand in the second future period would be lower than in the first future period. The peak water release occurs in July, when there is peak water demand. MS2 in the second future period showed the best performance in meeting water demand, with an average monthly water deficit of 38.88×10^6 m^3. MS1, MS4 and MS3 in the second future period have average

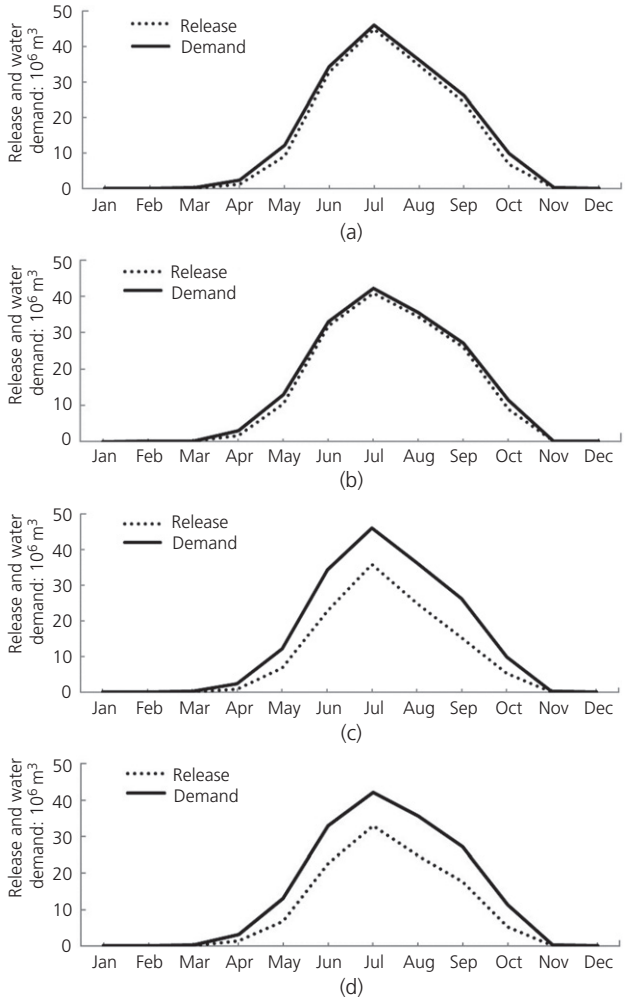

Figure 8. Long-term average monthly volume of water release and water demand for (a) MS1; (b) MS2; (c) MS3 and (d) MS4 (see Table 1) in the first future period and GHGES A2

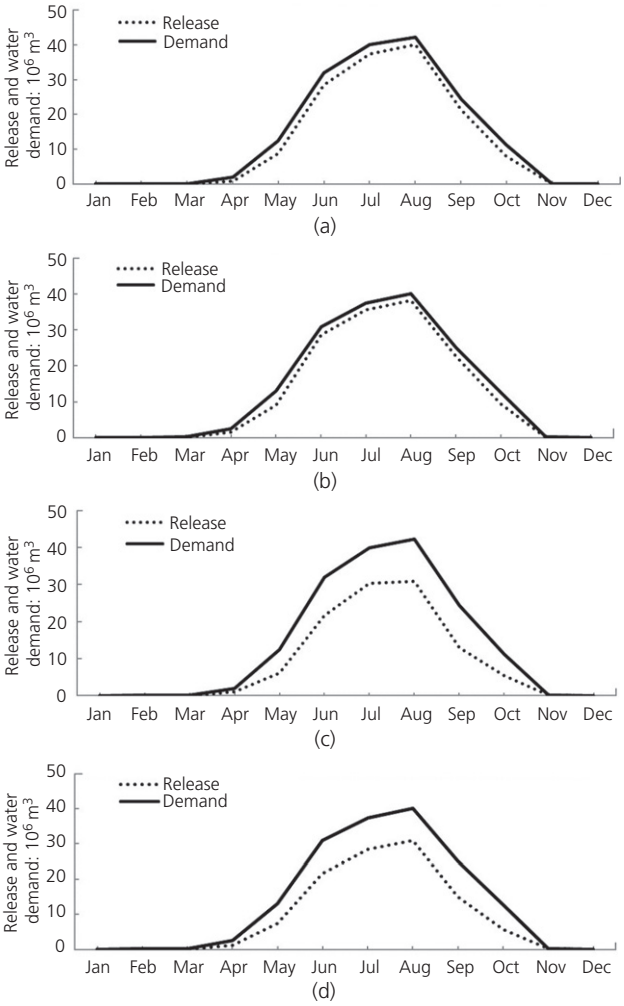

Figure 9. Long-term average monthly volume of water release and water demand for (a) MS5; (b) MS6; (c) MS7 and (d) MS8 (see Table 1) in the first future period and GHGES B2

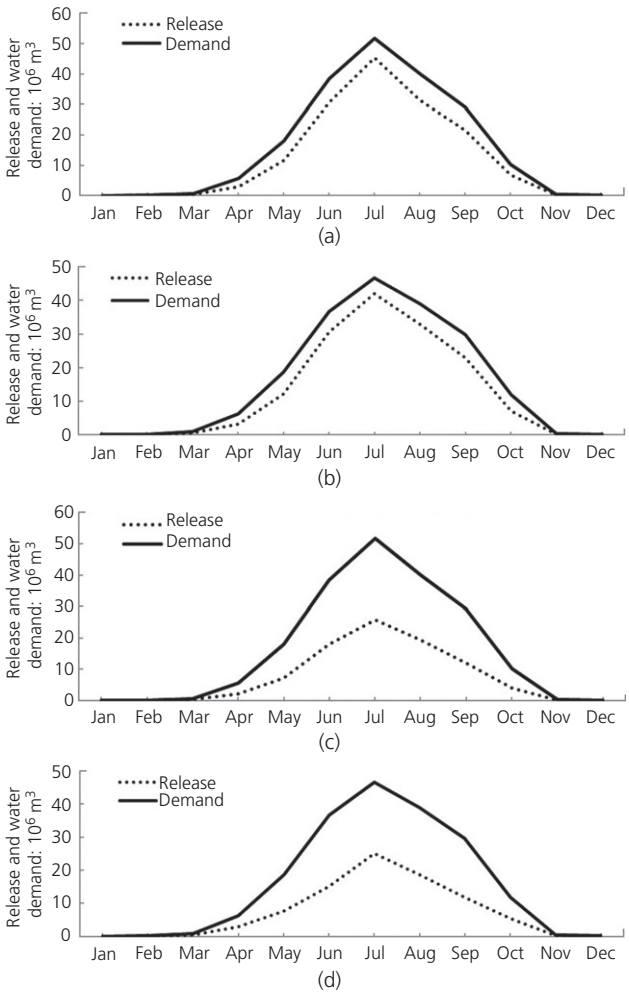

Figure 10. Long-term average monthly volume of water release and water demand for (a) MS1; (b) MS2; (c) MS3 and (d) MS4 (see Table 1) in the second future period and GHGES A2

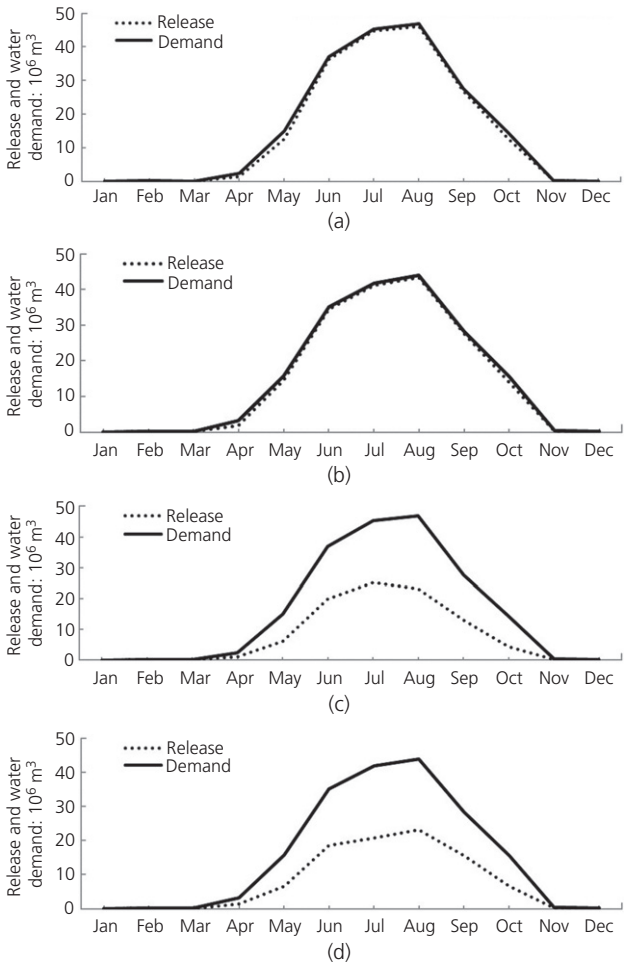

Figure 11. Long-term average monthly volume of water release and water demand for (a) MS5; (b) MS6; (c) MS7 (d) and MS8 (see Table 1) in the second future period and GHGES B2

monthly water deficits of 43.72×10^6 m^3, 10.66×10^6 m^3 and 107.27×10^6 m^3, respectively. The supply of demanded water improves with decreasing water deficit.

Figure 11 shows the average monthly reservoir water releases corresponding to MS5, MS6, MS7 and MS8 in the second future period under GHGES B2. MS6 is the best performing scenario with an average monthly water deficit of 7.50×10^6 m^3. The average monthly water deficits of MS5, MS8 and MS7 were found to be 8.08×10^6 m^3, 92.20×10^6 m^3 and 96.9×10^6 m^3, respectively.

The performance criteria for the eight modelling scenarios in the first and second future periods are compared in Tables 4 and 5, respectively. System performance was investigated by the performance criteria of reliability, resiliency and vulnerability. These measures explain how likely a system is to succeed in supplying water demand (reliability), how quickly it would recover from failure (resiliency) and how severe the consequences of failure may be (vulnerability). Table 4 shows that MS2 had the highest reliability (93.16%), the highest resiliency (38.41%) and the lowest vulnerability (6.82%), thus producing the best performance of the modelling scenarios insofar as future water supply is concerned. Table 5 shows that MS5 and MS6 respectively had reliabilities of 95.73% and 95.95%, resiliencies of 45.95% and 44.9%, and vulnerabilities of 4.27% and 4.5%; therefore, for the second future period, MS5 and MS6 exhibited the best performance in terms of future water supply.

Table 6 lists the calculated coefficients of variation (CoVs) for reservoir water deficits. The CoV is defined as the ratio of the standard deviation (σ) to the mean (μ) of reservoir water deficit. MS3 had the largest CoVs and thus the lowest uncertainty, whereas MS2 had the smallest CoVs and thus the lowest uncertainty.

Table 4. Comparison of performance criteria for the eight modelling scenarios in the first future period

Modelling scenario	Reliability: %	Resiliency: %	Vulnerability: %
MS1	91.91	30.18	8.09
MS2	93.18	38.41	6.82
MS3	66.51	17.44	33.49
MS4	67.31	17.73	32.69
MS5	88.08	22.22	11.92
MS6	89.58	27.59	10.42
MS7	65.92	17.71	34.08
MS8	67.87	18.37	32.13

Table 5. Comparison of efficiency criteria for the eight scenarios in the second future period

Modelling scenario	Reliability: %	Resiliency: %	Vulnerability: %
MS1	77.52	16.02	22.48
MS2	79.63	15.81	20.37
MS3	45.88	14.15	54.12
MS4	46.12	15.14	53.88
MS5	95.73	45.99	4.27
MS6	95.95	44.90	4.05
MS7	49.22	16.33	50.78
MS8	50.15	14.88	49.85

Table 6. CoVs corresponding to reservoir deficit

	CoV corresponding to reservoir deficit	
Modelling scenario	First future period (2040–2069)	Second future period (2070–2099)
MS1	1.01	0.98
MS2	0.94	0.89
MS3	1.08	1.12
MS4	1.02	1.09
MS5	0.95	1.08
MS6	0.99	0.93
MS7	1.07	1.12
MS8	1.01	1.10

4. Conclusions

This work evaluated the uncertainties of AOGCMs, GHGESs, models of estimation of reservoir inflow and methods for estimating future agricultural water demand in the Aidoghmoush basin located in northwestern Iran. The baseline period was taken as 1971–2000 and climate variables in two future periods (2040–2069 and 2070–2099) were simulated with six AOGCMs (under GHGESs A2 and B2). Projections of air temperature and precipitation for the future periods under both A2 and B2 were obtained and the average monthly temperature in the two future periods was found to increase relative to the baseline period. The average monthly temperature in future periods under A2 would be higher than the average monthly temperature under B2.

Estimates of future agricultural water demand with the FPM and HS methods revealed that the agricultural water demand would rise in future periods compared with the baseline period. It is noteworthy that water demand for agriculture depends on the area under cultivation and the irrigation requirement. The irrigation requirement depends directly and indirectly on climatic parameters. The projected water demand is therefore hydro-climatologic in nature.

Optimisation of reservoir operation with the PSO algorithm indicated that, in the first future period (2040–2069), the reservoir operation rule associated with the HS method and the ANN model (under GHGES A2) had the highest reliability (93.18%) and the lowest vulnerability (6.82%), and thus exhibited the best performance in supplying future agricultural water. In the second future period (2070–2099), reservoir operation corresponding to the HS method and the ANN model (under GHGES B2) showed the highest reliability (95.95%) and the lowest vulnerability (4.5%), thus producing the best reservoir operation rule in the second future period. MS2 had the lowest uncertainty and MS3 exhibited the highest uncertainty.

This study assessed the probable effects of climate change uncertainty on the effectiveness of reservoir operation policies for supplying future agricultural water use. Therefore, considering a general set of uncertainties in climate change studies as was done in this work can pave the way for the optimal use of available water.

Acknowledgement

The authors thank Iran's National Science Foundation for its financial support of this research.

REFERENCES

Abbaspour KC, Faramarzi M, Seyed Ghasemi S and Yang H (2009) Assessing the impact of climate change on water resources in Iran. *Water Resources Research* **45(10)**, https://doi.org/10.1029/2008WR007615.

Allen RG, Pereira LS, Raes D and Smith M (1998) *Crop Evapotranspiration. Guidelines for Computing Crop Water Requirements*. Food and Agricultural Organization, Rome, Italy, FAO Irrigation and Drainage Paper 56.

Allen RG, Walter IA, Elliot RL *et al.* (eds) (2005) *The ASCE Reference Evapotranspiration Equation*. ASCE, Reston, VA, USA.

Asgari HR, Bozorg-Haddad O, Pazoki M and Loáiciga HA (2016) Weed optimization algorithm for optimal reservoir operation. *Journal of Irrigation and Drainage Engineering* **142(2)**: 04015055, https://doi.org/10.1061/(ASCE)IR.1943-4774.0000963.

Ashofteh PS (2015) *Developing Flexible Strategies in Water Resources and Consumption for Adaptation with Climate Change*. PhD dissertation, University of Tehran, Tehran, Iran.

Ashofteh PS, Bozorg-Haddad O and Mariño MA (2014) Discussion of 'Estimating the effects of climatic variability and human activities on streamflow in the Hutuo River basin'. *Journal of Hydrologic Engineering* **19(4)**: 836–836.

Ashofteh PS, Bozorg-Haddad O and Mariño MA (2015) Risk analysis of water demand for agricultural crops under climate change. *Journal of Hydrologic Engineering* **20(4)**, https://doi.org/10.1061/(ASCE)HE.1943-5584.0001053.

Ashofteh PS, Bozorg-Haddad O and Loáiciga HA (2017) Development of adaptive strategies for irrigation water demand management under climate change. *Journal of Irrigation and Drainage Engineering* **143(2)**, https://doi.org/10.1061/(ASCE)IR.1943-4774.0001123.

Baede APM, Ahlonsou E, Ding Y and Schimel DS (2001) The climate system: an overview. In *Climate Change 2001: Impacts, Adaptation and Vulnerability* (McCarthy JJ, Canziani OF, Leary NA, Dokken DJ and White KS (eds)). Cambridge University Press, Cambridge, UK, pp. 87–98.

Bani-Habib M, Moosavi SM and Jamali FS (2010) An artificial neural network model detecting daily correlation among the stations in reservoir inflow forecasting. *Iranian Water Research Journal* **4(7)**: 25–32.

Besaw LE, Rizzo DM, Bierman PR and Hackett WR (2010) Advances in ungauged streamflow prediction using artificial neural networks. *Journal of Hydrology* **386(1)**: 27–37.

Croke BFW, Andrews F, Spate J and Cuddy S (2005) *IHACRES User Guide*. 2nd edn. iCAM, School of Resources, Environment and Society, The Australian National University, Canberra, Australia, Technical Report 2005/19. See http://www.toolkit.net.au/ihacres (accessed 26/01/2021).

Doorenbos J and Pruitt WO (1984) *Guidelines for Predicting Crop Water Requirements*. Food and Agricultural Organization, Rome, Italy, FAO Irrigation and Drainage Paper 24.

Fallah-Mehdipour E, Bozorg-Haddad O and Mariño MA (2014) Genetic programming in groundwater modeling. *Journal of Hydrologic Engineering* **19(12)**: 04014031.

FAO (Food and Agricultural Organization) (1998) *Crop Evapotranspiration – Guidelines for Computing Crop Water Requirements*. FAO, Rome, Italy, FAO Irrigation and Drainage Paper 56.

Farhangi M (2010) *Investigating the Effect of Discharge Uncertainty on the Operation of the Reservoir System*. Master's dissertation, University of Tehran, Tehran, Iran.

Hargreaves GH and Samani ZA (1985) Reference crop evapotranspiration from temperature. *Applied Engineering in Agriculture* **1(2)**: 96–99.

IPCC (Intergovernmental Panel on Climate Change) (2001) *Climate Change 2001: IPCC Third Assessment Report*. IPCC Secretariat, Geneva, Switzerland.

Jahandideh-Tehrani M, Bozorg-Haddad O and Loáiciga HA (2015) Hydropower reservoir management under climate change: the Karoon reservoir system. *Water Resources Management* **29(3)**: 749–770.

Jakeman AJ and Hornberger GM (1993) How much complexity is warranted in a rainfall-runoff model? *Water Resources Research* **29(8)**: 2637–2649.

Jensen ME (1974) *Consumptive Use of Water and Irrigation Water Requirements*. ASCE, New York, NY, USA.

Kennedy J and Eberhart R (1995) Particle swarm optimization. *Proceedings of IEEE International Conference on Neural Networks, Perth, Australia*. IEEE, Piscataway, NJ, USA, pp. 1942–1948.

Li L, Xu H, Chen X and Simonovic SP (2010) Streamflow forecast and reservoir operation performance assessment under climate change. *Water Resources Management* **24(1)**: 83–104.

Loáiciga HA, Maidment D and Valdes JB (2000) Climate change impacts in a regional karst aquifer, Texas, USA. *Journal of Hydrology* **227(1–4)**: 173–194.

Masood M and Takeuchi K (2016) Climate change impacts and its implications on future water resource management in the Meghna basin. *Futures* **78–79**: 1–18, https://doi.org/10.1016/j.futures.2016.03.001.

McIntyre N and Al-Qurashi A (2009) Performance of ten rainfall-runoff models applied to an arid catchment in Oman. *Environmental Modelling & Software* **24(6)**: 726–738.

Minville M, Brissette F and Leconte R (2008) Uncertainty of the impact of climate change on the hydrology of a Nordic watershed. *Journal of Hydrology* **358(1)**: 70–83.

Pachauri RK and Reisinger A (eds) (2007) *Climate Change 2007: Synthesis Report. Contribution of Working Groups I, II and III to the Fourth Assessment Report*. Intergovernmental Panel on Climate Change, Geneva, Switzerland.

Penman HL (1956) Evaporation: an introductory survey. *Netherlands Journal of Agricultural Sciences* **4(1)**: 9–29.

Smith M (1992) *CROPWAT: A Computer Program for Irrigation Planning and Management*. Food and Agricultural Organization, Rome, Italy, FAO Irrigation and Drainage Paper 46.

Soltanjalili M, Bozorg-Haddad O and Mariño MA (2011) Effect of breakage level one in design of water distribution networks. *Water Resources Management* **25(1)**: 311–337, https://doi.org/10.1007/s11269-010-9701-1.

Thornthwaite CW (1948) An approach toward a rational classification of climate. *Geographical Review* **38(1)**: 55–94.

Warren AJ and Holman IP (2012) Evaluating the effects of climate change on the water resources for the city of Birmingham, UK. *Water and Environment Journal* **26(3)**: 361–370.

Wilby RL and Harris I (2006) A framework for assessing uncertainties in climate change impacts: low-flow scenario for the River Thames, UK. *Water Resources Research* **42(2)**, https://doi.org/10.1029/2005WR004065.

Xing-Guo M, Shi H, Zhong-Hui L, Su-Xia L and Jun X (2017) Impacts of climate change on agricultural water resources and adaptation on the North China Plain. *Advances in Climate Change Research* **8(2)**: 93–98.

How can you contribute?

To discuss this paper, please email up to 500 words to the editor at journals@ice.org.uk. Your contribution will be forwarded to the author(s) for a reply and, if considered appropriate by the editorial board, it will be published as discussion in a future issue of the journal.

Proceedings journals rely entirely on contributions from the civil engineering profession (and allied disciplines). Information about how to submit your paper online is available at www.icevirtuallibrary.com/page/authors, where you will also find detailed author guidelines.